Appl. Phys. A 86, 315–319 (2007)
DOI: 10.1007/s00339-006-3796-5

Applied Physics A
Materials Science & Processing

Rapid communication

H.W. KIM

Temperature-controlled synthesis of Ga_2O_3 nanobelts and nanosheets

School of Materials Science and Engineering, Inha University, Incheon 402-751, South Korea

Received: 6 November 2006/Accepted: 16 November 2006
Published online: 8 December 2006 • **© Springer-Verlag 2006**

ABSTRACT We have investigated the effect of growth temperature on structural morphology and photoluminescence (PL) properties of as-synthesized gallium oxide (Ga_2O_3) nanostructures. The products consisted of Ga_2O_3 nanobelts and nanosheets (i.e. wider nanobelts), which had monoclinic crystalline structures. The average width of structures grown at 1000 °C was relatively greater than those at 800 °C, revealing that higher temperature favored the formation of nanosheets. PL measurements of 800 °C- and 1000 °C-grown samples indicated that both samples exhibited a broad emission band peaked around the blue-light region, while only the 800 °C-grown sample showed a red peak.

PACS 81.07.-b; 81.05.Je; 61.10.Nz; 68.37.Hk; 68.37.Lp

1 Introduction

Gallium oxide (Ga_2O_3) is a stable wide-band-gap compound with intense luminescence properties [1]. Inorganic materials with different morphologies and sizes can exhibit different properties [2], even if they are made up of the same elements. Accordingly, various structural and morphological forms of Ga_2O_3 materials have been fabricated over the past several years. Among them, low-dimensional structures including nanowires [3–5], nanobelts, and nanosheets [6, 7] are supposed to have potential applications to nanoelectronics and optoelectronics, owing to their novel physical properties.

While the growth behavior of film-like structures is strongly dependent on the growth temperature, the effect of the temperature on the growth of low-dimensional nanostructures has been less studied. Variation of wire shapes depending on growth temperature was reported from Si [8, 9], SiO_x [10], and ZnO nanowires [11]. Temperature-induced changes in product morphology among nanowires and clusters were reported from WO_3 nanomaterials by the colloidal gas aphron method [12] and tri(8-hydroquinoline)aluminum nanomaterials via physical vapor deposition [13]. In the present communication, we report the effect of growth temperature on the characteristics of Ga_2O_3 nanostructures deposited by thermal evaporation of GaN powders. Although there have been reports of the simultaneous production of nanobelts and nanosheets [6, 7, 14], to the best of our knowledge this is the first report of the temperature-induced morphological changes in the product comprising nanobelts and nanosheets. We discuss the possible growth mechanism. We also have investigated the structural and photoluminescence (PL) properties of the as-prepared Ga_2O_3 nanostructures. Controlling the morphology of the nanostructures is an important step not only for scientific interests but also toward design and applications of nanostructures.

2 Experimental

The experimental apparatus was previously described [15]. We have employed Au-coated Si substrates, in which a layer of Au (about 150 nm) was deposited by radio-frequency magnetron sputtering. The 99.9%-pure GaN powders and the substrates, respectively, were placed on the lower and the upper holder in the center of the quartz tube inserted into a vertical furnace. The powder-to-substrate distance was 5 mm. Since our objective was to investigate the effect of growth temperature, the substrate temperature was set to 800 °C, 900 °C, and 1000 °C for 2 h in a flow of nitrogen (N_2) gas (flow rate: 500 standard cm^3/min). The oxygen was unintentionally introduced by the residual O_2 in the N_2 gas. After deposition, each substrate was covered with a layer of the product. The as-grown samples were subsequently examined by grazing angle (0.5°) X-ray diffraction (XRD, Rigaku DMAX 2500) with Cu K_{α_1} radiation ($\lambda = 0.154056$ nm), scanning electron microscopy (SEM, Hitachi S-4200), and transmission electron microscopy (TEM, Philips CM-200) with energy-dispersive X-ray spectroscopy (EDX) installed. The PL measurement was performed at room temperature using a He-Cd laser line of 325 nm as the excitation source.

3 Results and discussion

Figure 1a–c show the typical top-view SEM images of the products

✉ Fax: +82-32-860-7544, E-mail: hwkim@inha.ac.kr

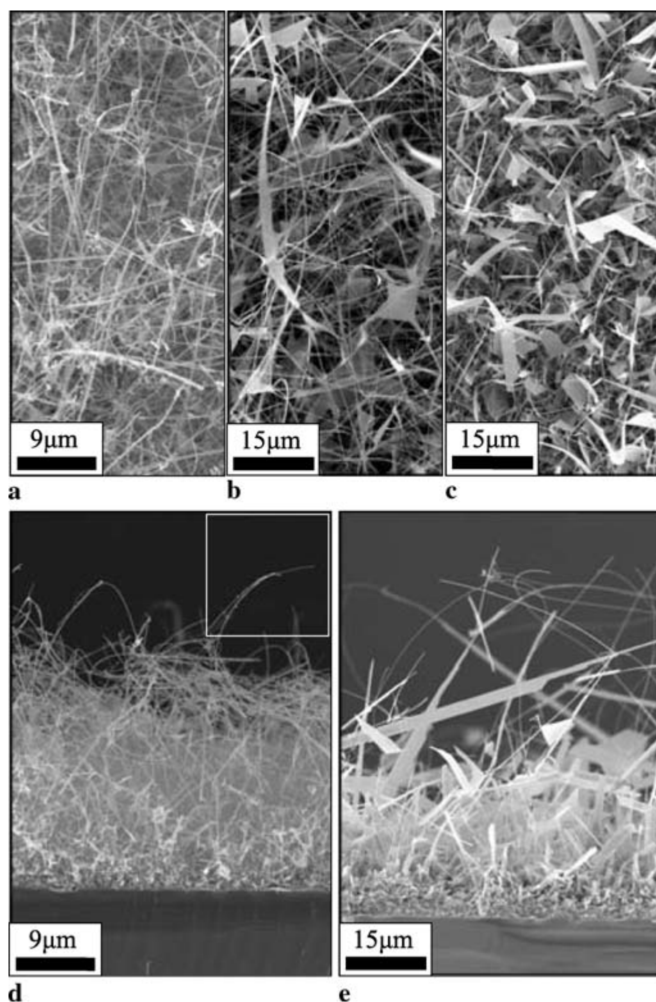

FIGURE 1 Top-view SEM images of the products grown at (**a**) 800 °C, (**b**) 900 °C, and (**c**) 1000 °C. Side-view SEM images of the products grown at (**d**) 800 °C and (**e**) 1000 °C. *Upper right inset* in (**d**) shows the tip part of a 1D nanostructure grown at 800 °C

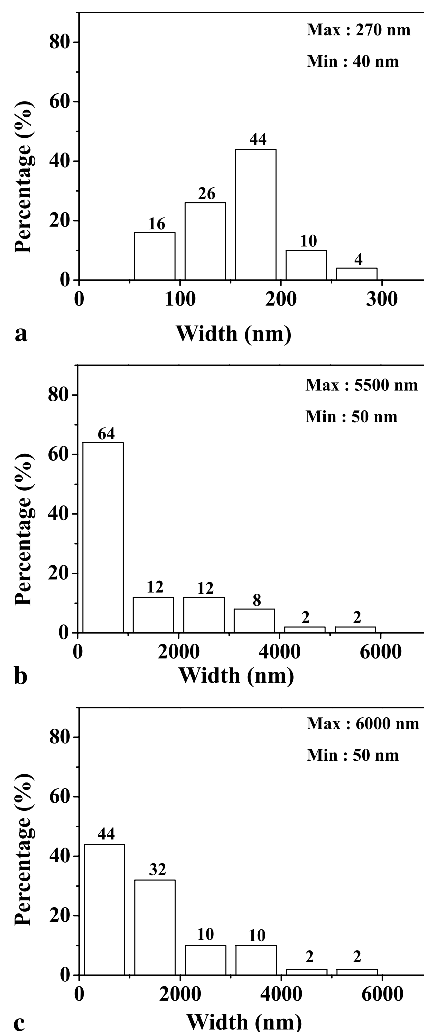

FIGURE 2 The width distributions of the products grown at (**a**) 800 °C, (**b**) 900 °C, and (**c**) 1000 °C

grown at 800, 900, and 1000 °C, respectively. We estimate that while the product grown at 800 °C mainly consists of relatively thin one-dimensional (1D) nanostructures, the products grown at 900 °C and 1000 °C consist of thin 1D nanostructures with some additional wider structures. Figure 1d and e show the typical side-view SEM images of the products grown at 800 and 1000 °C, respectively, apparently revealing that the average width (or diameter) of the structures grown at 1000 °C is relatively greater than those at 800 °C. The upper right inset in Fig. 1d reveals that no catalyst particle can be seen at the tip of a 1D structure grown at 800 °C. Statistical analysis of many SEM images indicated that the width of the Ga_2O_3 structures produced with the growth temperatures of 800, 900, and 1000 °C, respectively, were in the range of 40–270 nm, 50 nm–5.5 µm, and 50 nm–6 µm, respectively. The width distributions of the products grown at 800, 900, and 1000 °C are shown in Fig. 2a–c. By comparing Fig. 2c with Fig. 2b, we reveal that approximately 64 and 44% of the products have widths below 1000 nm, respectively, for the samples grown at 900 and 1000 °C. The width distribution analysis suggests that the average width of the products increases with increasing growth temperature in the range of 800–1000 °C, agreeing with SEM images (Fig. 1).

Figure 3 shows the typical XRD pattern of the products. All recognizable reflection peaks can be well indexed to the monoclinic β-Ga_2O_3 structure (JCPDS: 11-0370). No reflection peaks from the impurities, such as unreacted Ga or other gallium oxides, were observed, indicating the high purity of the products. Since the XRD spectrum was not dependent on the growth temperature, we reveal that products are pure Ga_2O_3 phase, whether they are close to sheet-type or belt-like morphology.

For obtaining more detailed information about the individual nanostructures, we have carried out TEM analysis. Figure 4a is a low-magnification TEM image of the products grown at 800 °C. The ripple-like contrast of the belts in the TEM image was presumably due to the bend contours, as typically observed in the TEM observation of slightly bent thin crystals. No spherical droplets or nanoparticles can be seen at tips of the nanobelts. The EDX analysis indicated that the 1D nanostructures were composed of the elements Ga and O, regardless of position from the stem to the ends (not shown here). Figure 4b exhibits a TEM image of a single nanobelt with a width of about 40 nm. The inset in Fig. 4b

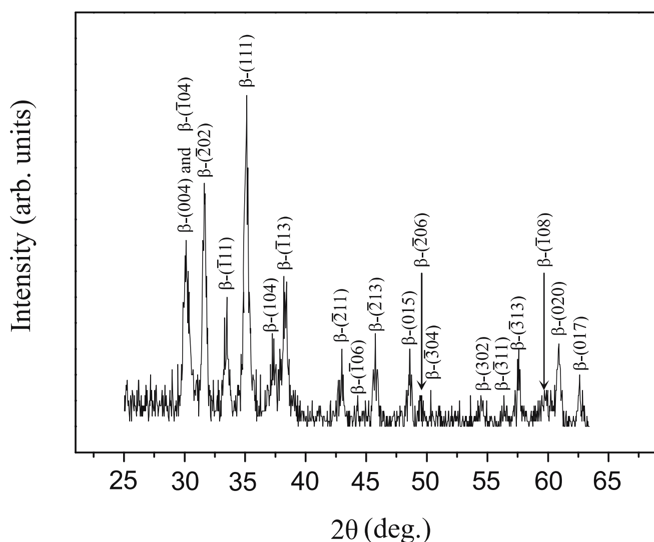

FIGURE 3 XRD patterns recorded from the products

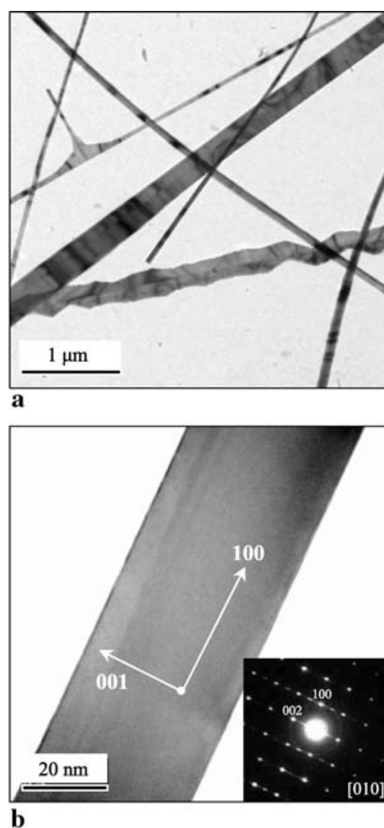

FIGURE 4 (**a**) Low-magnification TEM image of the product grown at 800 °C. (**b**) TEM image of a single β-Ga_2O_3 nanobelt (*inset*: corresponding SAED pattern recorded along the [010] zone axis)

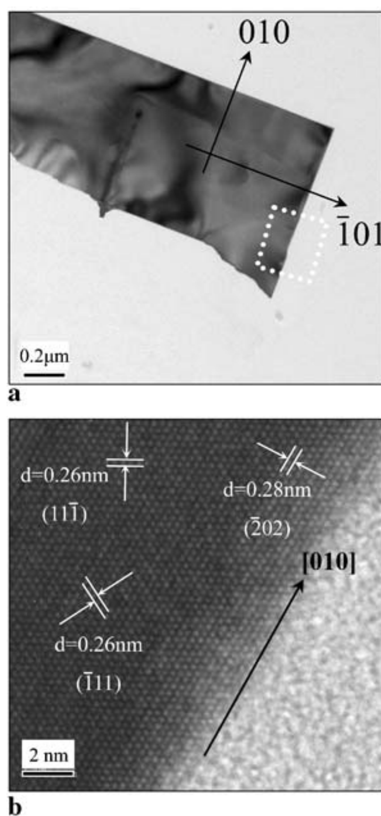

FIGURE 5 (**a**) Low-magnification TEM image of a piece of a wide structure grown at 1000 °C. (**b**) HRTEM image corresponding to an area enclosed by the *square* in (**a**)

shows an associated selected area electron diffraction (SAED) pattern. The SAED pattern, recorded perpendicular to the nanobelt long axis, can be indexed for the [010] zone axis of crystalline β-Ga_2O_3. On the basis of careful analysis of the diffraction pattern, we determined the top-view lattice plane, the side-view lattice plane, and the plane perpendicular to the growth direction, respectively, to be (010), (001), and (100) lattice planes.

Figure 5a shows a low-magnification TEM image of a piece of a wide nanostructure grown at 1000 °C. We surmise that such a nanostructure may not be firm and easily broken by ultrasonic waves while preparing the TEM specimens. Since the unbroken corner of the TEM sample is rectangular in shape, we deduce that the original shape of the structure corresponds to wide nanobelts or nanosheets shown in Fig. 1c and e. The length direction is supposed to be along the [010] or [$\bar{1}$01] direction, as shown in Fig. 5a. Figure 5b is a high-resolution TEM (HRTEM) image enlarging an area enclosed by the square in Fig. 5a, revealing a good crystallinity. The interplanar spacings are about 0.28 nm, 0.26 nm, and 0.26 nm, respectively, corresponding to ($\bar{2}$02), (11$\bar{1}$), and ($\bar{1}$11) planes of monoclinic β-Ga_2O_3.

There are two well-accepted mechanisms for the growth of 1D nanostructures, the vapor–liquid–solid (VLS) and the vapor–solid (VS) mechanisms. The most remarkable sign of the VLS mechanism is that the solidified droplet, which acts as liquid-forming agent, can be observed at the ends of the structures. In the present study, in spite of employing the Au-coated substrate, there was no evidence of Au catalyst being present on the ends of the nanobelts from SEM and TEM analyses. It indicates that the Ga_2O_3 nanobelts are more likely to be produced via a VS mechanism than the conventional tip-growth VLS one. In addition, the other possibility may lie in the base-growth mechanism. In this type of extended VLS process, the Au catalytic particles may stay at root parts of the nanobelts during the growth process. Similarly, previous work on the synthesis of gallium nitride nanorods [16] and carbon nanotubes [17] revealed that the growth can be ascribed to the base-growth mechanism, in which the metal catalyst remained situated at the bottom of the nanostructures. With the formation process being controlled by kinetics during crystal growth, Ga vapor generated from the GaN powders combines with oxygen to produce Ga_2O_3 nanostructures in the present vapor-phase-involved reaction system. The two-dimensional (2D) nucleation probability on the surface of a whisker was estimated to be proportional to $\exp(-\pi\sigma^2/(k^2T^2 \ln\alpha))$, where σ is the surface energy of the solid whisker, k is the Boltzmann con-

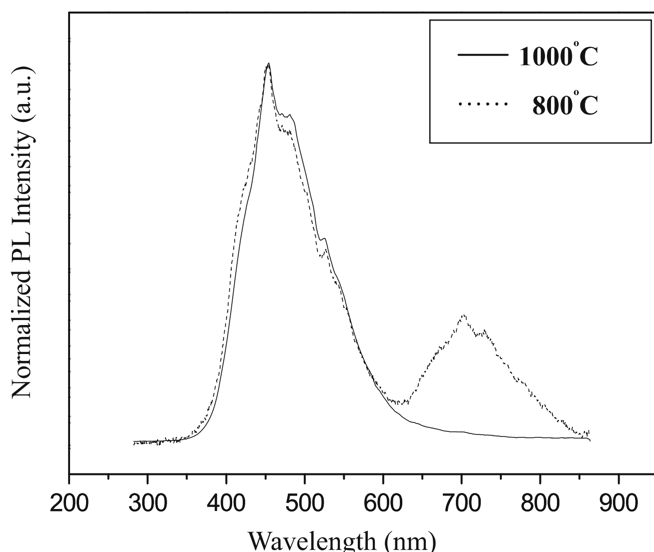

FIGURE 6 Room-temperature PL spectra with an excitation wavelength at 325 nm for the samples grown at (**a**) 800 °C and (**b**) 1000 °C

stant, T is the absolute temperature, and α is the supersaturation ratio determined by $\alpha = p/p_0$ (usually $\alpha > 1$), in which p is the actual vapor pressure and p_0 the equilibrium vapor pressure according to temperature T [18]. With the parameters such as supersaturation ratio (α) and surface energy (σ) being less affected by temperature, we suppose that the nucleation density is approximately proportional to $\exp(-T^{-2})$. Therefore, according to the above equation, high temperature facilitates the 2D nucleation, resulting in the preferred formation of the wider belt-like or sheet-like structure. Further study is in progress to reveal the detailed growth mechanism of sheet-like structures. In contrast, lower temperature promotes the growth of thin 1D structures, which correspond to the relatively narrow nanobelts.

The PL spectrum at room temperature is shown in Fig. 6. There is an apparent broad, strong emission PL band, which can be a superimposition of several peaks. The blue emission peak centered at around 453 nm with a shoulder peak at around 481 nm is known to be associated with vacancies in Ga_2O_3 [19, 20]. Similarly, blue emission bands peaked in the range of 410–480 nm have been frequently reported in the case of Ga_2O_3 nanowires [4, 21, 22] and nanobelts [23]. According to Binet and Gourier [24], an electron in a donor is captured by a hole in an acceptor to form a trapped exciton, which recombines radiatively and emits a blue photon. The green shoulder peak centered at around 524 nm may correspond to a defect level with a different recombination mechanism [25]. In the sample grown at 800 °C, we observe an additional red peak centered at around 701 nm, arising from intrinsic impurities or nitrogen incorporation during the evaporation process under the N_2 gas flow [25]. It is noteworthy that we do not clearly observe the red peak in the samples grown at a higher temperature of 1000 °C. It has been reported that the nitrogen incorporation or content in Ga-containing compounds increased with decreasing growth temperature [26, 27]: from the kinetic model, at low growth temperatures, it is assumed that the rate of nitrogen desorption is low compared with the rate of adsorption, resulting in the increased nitrogen incorporation. By a similar model, we suppose that more nitrogen has been incorporated into the Ga_2O_3 nanostructures at a lower growth temperature of 800 °C, resulting in the noticeable observation of the red peak from the PL spectrum.

4 Conclusions

We successfully fabricated single-crystalline Ga_2O_3 nanobelts and nanosheets on an Au-coated Si substrate via a thermal evaporation method of heating GaN powders under N_2 flow. While the 800 °C-grown product consists of 1D nanostructures with relatively smaller width, the 1000 °C-grown product additionally comprises the structures which are close to wider sheet-like structures, suggesting that morphology of the Ga_2O_3 nanostructures can be controlled by choosing the substrate temperature. Not only nanobelts but also nanosheets have a monoclinic β-Ga_2O_3 structure. We speculate about the mechanism by which temperature affects the morphology; this needs deep study in the future. While the PL spectra of 800 °C- and 1000 °C-grown samples commonly exhibit the blue emission, the additional red peak is clearly observed in the 800 °C-grown sample. We have discussed the possible PL emission mechanisms.

ACKNOWLEDGEMENTS This work was supported by an Inha University Research grant.

REFERENCES

1 Z.W. Pan, Z.R. Dai, Z.L. Wang, Science **291**, 1947 (2001)
2 J. Hulliger, Angew. Chem. Int. Edit. **33**, 143 (1994)
3 Y.C. Choi, W.S. Kim, Y.S. Park, S.M. Lee, D.J. Bae, Y.H. Lee, G.S. Park, W.B. Choi, N.S. Lee, J.M. Kim, Adv. Mater. **12**, 746 (2000)
4 C.H. Liang, G.W. Meng, G.Z. Wang, Y.W. Wang, L.D. Zhang, S.Y. Zhang, Appl. Phys. Lett. **78**, 3202 (2001)
5 G. Gundiah, A. Govindaraj, C.N.R. Rao, Chem. Phys. Lett. **351**, 189 (2002)
6 Z.R. Dai, Z.W. Pan, Z.L. Wang, J. Phys. Chem. B **106**, 902 (2002)
7 X. Xiang, C.B. Cao, Y.J. Guo, H.S. Zhu, Chem. Phys. Lett. **378**, 660 (2003)
8 Y.Q. Chen, K. Zhang, B. Miao, B. Wang, J.G. Hu, Chem. Phys. Lett. **358**, 396 (2002)
9 Z.W. Pan, Z.R. Dai, L. Xu, S.T. Lee, Z.L. Wang, J. Phys. Chem. B **105**, 2507 (2001)
10 Z. Pan, S. Dai, D.B. Beach, D.H. Lowndes, Nano Lett. **3**, 1279 (2003)
11 X.Q. Meng, D.X. Zhao, J.Y. Zhang, D.Z. Shen, Y.M. Lu, Y.C. Liu, X.W. Fan, Chem. Phys. Lett. **407**, 91 (2005)
12 S.F. Abdullah, S. Radiman, M.A.A. Hamid, N.B. Ibrahim, Colloid Surf. A **280**, 88 (2006)
13 X. Tian, J. Fei, Z. Pi, C. Yang, D. Luo, F. Pei, L. Zhang, Solid State Commun. **138**, 530 (2006)
14 C. Liang, Y. Shimizu, T. Sasaki, H. Umehara, N. Koshizaki, J. Phys. Chem. B **108**, 9728 (2004)
15 N.H. Kim, H.W. Kim, Appl. Surf. Sci. **242**, 29 (2005)
16 W.-Q. Han, A. Zettl, Appl. Phys. Lett. **80**, 303 (2002)
17 S. Fan, M.G. Chapline, N.R. Franklin, T.W. Tombler, A.M. Cassell, H. Dai, Science **283**, 512 (1999)
18 Z.R. Dai, Z.W. Pan, Z.L. Wang, Adv. Funct. Mater. **13**, 9 (2003)

19 T. Harwig, F. Kellendouk, J. Solid State Chem. **24**, 255 (1978)
20 V.I. Vasil'tsiv, Y.M. Zakharko, Y.I. Prim, Ukr. Fiz. Zh. **33**, 1320 (1988)
21 D.P. Yu, J.-L. Bubendorff, J.F. Zhou, Y. Leprince-Wang, M. Troyon, Solid State Commun. **124**, 417 (2002)
22 J. Zhang, F. Jiang, Chem. Phys. **289**, 243 (2003)
23 L. Fu, Y. Liu, P. Hu, K. Xiao, G. Yu, D. Zhou, Chem. Mater. **15**, 4287 (2003)
24 L. Binet, D. Gourier, J. Phys. Chem. Solids **59**, 1241 (1998)
25 Y.P. Song, H.Z. Zhang, C. Lin, Y.W. Zhu, G.H. Li, F.H. Yang, D.P. Yu, Phys. Rev. B **69**, 075 304 (2004)
26 H. Dumont, L. Auvray, Y. Monteil, J. Bouix, Mater. Sci. Eng. B **84**, 258 (2001)
27 D.J. Friedman, J.F. Geisz, S.R. Kurtz, J.M. Olson, R. Reedy, J. Cryst. Growth **195**, 438 (1998)